Available online at www.sciencedirect.com
SCIENCE DIRECT
Cement and Concrete Research 36 (2006) 71–78
Cement and Concrete Research

Chemical structure of cement aged at normal and elevated temperatures and pressures Part I. Class G oilwell cement

Gwenn Le Saout[a,b,*], Eric Lécolier[a], Alain Rivereau[a], Hélène Zanni[b]

[a]Institut Français du Pétrole, 1-4 av de Bois Préau, 92852 Rueil-Malmaison, France
[b]Laboratoire de Physique et Mécanique des Milieux Hétérogènes UMR CNRS 7636, Ecole Supérieure de Physique et Chimie Industrielles, 10 rue Vauquelin, 75231 Paris Cedex 05, France

Received 3 March 2004; accepted 21 September 2004

Abstract

The prime objective of the plug-and-abandon operations is to provide zonal isolation for infinite time. Cement-based materials are generally used as plugging materials. Therefore, it is important to understand the physical and chemical processes causing cement degradation in the downhole environment. In this study, we have characterised a Class G oilwell cement immersed for 1 year in brine at T=293 K, p=10^5 Pa and T=353 K, p=7×10^6 Pa using NMR and XRD techniques. In order to have a better understanding of the ^{27}Al NMR spectra, selective dissolution has been performed. The results show that after 1 year of immersion in brine at T=293 K, p=10^5 Pa, monosulfate is converted to Friedel's salt. Leaching resulted in the disappearance of portlandite and the formation of calcite and a more polymerised calcium silicate hydrates (C–S–H). In the T=353 K, p=7×10^6 Pa mineralogy, ettringite is converted to hydrogrossular.

Keywords: Temperature; X-ray scattering; NMR; Aging; Oilwell cement

1. Introduction

Cement-based materials are used in the oil and gas industry for cementing oilwells. The main role of the cement sheath is to permanently isolate all subsurface formations penetrated by the well [1]. This permanent isolation is expected not only during the oil production but also after the plugging of the wells. In any case, durability of the cement-based materials placed within the wells is of utmost importance. To reach this target, many formulations have been developed for oilwell cementing, but only a few studies have been devoted to the physical and chemical processes causing cement degradation under downhole conditions [2–5].

The objective of this work is to study the structure and the properties of Class G oilwell cement. X-ray diffraction (XRD) allows us to investigate the highly crystallized phases, whereas nuclear magnetic resonance (NMR) is very adapted to the study of amorphous as well as crystalline materials. Previous structural characterisations of this system cured 30 days in tap water at T=293 K, p=10^5 Pa and T=353 K, p=7×10^6 Pa revealed that an increase of pressure and temperature lead to a more polymerised calcium silicate hydrates (C–S–H) [6]. We present in this study the investigation of the microstructure of these samples exposed to brine during 1 year.

2. Background: oilwell cementing

Rotary drilling is the worldwide method used to drill oil and gas wells. This method consists in the use of a rotating

* Corresponding author. Laboratoire de Physique et Mécanique des Milieux Hétérogènes UMR CNRS 7636, Ecole Supérieure de Physique et Chimie Industrielles, 10 rue Vauquelin, 75231 Paris Cedex 05, France. Tel.: +33 1 40 79 45 56; fax: +33 1 40 79 47 95.
E-mail address: lesaout_gwenn@yahoo.fr (G. Le Saout).

0008-8846/$ - see front matter © 2004 Elsevier Ltd. All rights reserved.
doi:10.1016/j.cemconres.2004.09.018

bit which crushes the rock formation, and a continuous injection of drilling fluid, which removes the rock cuttings and brings them to the surface. One of the main advantages of the rotary method is that the drilling fluid can be pumped through the bit. Once a section of the well has been drilled, the drill pipe is removed from the hole and a casing pipe is run into the hole until it reaches the bottom. This operation is achieved with the borehole full of drilling fluid. Once the casing pipe is in place, a cement slurry is pumped down into the casing string to the bottom of the well and then flows up through the annulus between the casing and the borehole wall where it sets. This last operation is called primary cementing. The major goal of the primary cementing is to provide a complete and permanent zonal isolation within the well bore. This means that the cement sheath must prevent any fluid circulation (gas, oil, water, ...) between different rocks layers. Incomplete zonal isolation may lead to environmental pollution problems or production rates lower than expected. That is why primary cementing is often considered as one of the most important operations performed in a well. Primary cementing also aims at mechanically securing the casing string to the borehole walls and at protecting the casing from corrosion by the fluids contained in the drilled rock formations.

After 25 years or so, when the production rate becomes very low, the wells have to be plugged. The main aim of well abandonment is to permanently seal the well bore for a geological time scale in order to prevent any leakage of formation fluids to surface. Long-term durability of the cement is of paramount importance in this operation to guarantee the tightness of the plugged wells. However, in North America, there are literally tens of thousands of abandoned oil and gas wells, including gas storage wells that currently leak gas to surface. Much of this gas enters the atmosphere directly, contributing slightly to the green-house effect. Some of the gas enters shallow aquifers, where trace of sulphurous compounds can render the water nonpotable [7].

3. Experimental details

The Class G Portland cement was obtained from the Dyckerhoff company (Bogue composition (wt.%) : 51.2 C_3S, 27 C_2S, 2.3 C_3A, 14.4 C_4AF; for determination of potential composition for a Class G oilwell, see Ref. [8] and references therein) and was made with a water cement ratio w/c=0.44. Specimens were cast in rectangular moulds (2×2×30 cm) and were hardened in slightly hard tap water (2.9×10^{-3} M $CaCO_3$) for 30 days with two curing temperature and pressure conditions: T=293 K, p=10^5 Pa (samples labelled CI in the text) and T=353 K, p=7×10^6 Pa (CII). Specimens were demoulded and 2×10^{-2} m cubes were cut from the bars before being placed in the brine media up to 1 year with the two curing temperature and pressure conditions. The volume ratio of the brine to the volume of the material was 1:10 and the brine was renewed monthly. Table 1 shows the chemical composition of brine employed for the leaching test which has neutral pH and is approximately 0.35 M NaCl with other minor components. After 1 year, chemical analyses were made on the superficial layer of typically 200–300 μm which was in contact with brine and on the bulk sample.

X-ray diffraction data were collected using a Philips PW 1820 diffractomer employing the $Cu_{K\alpha}$ radiation (λ_0= 0.154 nm). The samples were scanned at 0.6° per minute between 5 and 65° 2θ.

The ^{29}Si NMR spectra were carried out on a Bruker ASX 300 spectrometer (7.05 T magnetic field) at 59.6 MHz. Spectra were recorded at 7 kHz spinning rate in 4 mm ZrO_2 rotors. Single pulse experiments without ^{1}H decoupling were carried out by applying 90° pulses with recycle delay of 8 s in order to respect the relaxation times of the species present in the samples. The ^{29}Si chemical shift of the peaks were analysed using the Q_n(mAl) classification where the Si tetrahedron is connected to m Al and ($n-m$) Si tetrahedra where n=0 to 4 and m=0 to n. In aluminosilicates, the shifts are further influenced by the replacement of Si by Al in tetrahedra adjacent to a given Si site, generally producing down-field shifts of 3–5 ppm/Al [9]. The ^{27}Al NMR experiments were performed on a Bruker ASX 500 spectrometer, in a 11.7 T field, operating at 129.80 MHz for ^{27}Al. Spectra were recorded at 25 kHz spinning rate in 2.5 mm ZrO_2 rotors. All experiments employed single pulse (π/12) excitation width pulse of τ_p=0.5 μs without ^{1}H decoupling and a 1 s relaxation delay. The ^{27}Al and ^{29}Si chemical shifts were respectively referenced relative to a 1.0 M $AlCl_3$–$6H_2O$ solution and to tetramethylsilane $Si(CH_3)_4$ (TMS) at 0 ppm, using $Si[(CH_3)_3]_8Si_8O_{20}$ (Q8M8) as a secondary reference (the major peak being at 11.6 ppm relatively to TMS).

4. Results

4.1. X-ray diffraction

Phases identification of hardened cements after a 30-day cure at ambient temperature and atmospheric pressure by XRD analysis (Fig. 1a) shows the presence of unhydrated phases alite C_3S, belite C_2S, ferrite phase C_4AF and the

Table 1
Chemical composition of brine employed for the leaching test

Ionic species	Cl^-	Na^+	K^+	HCO_3^-	SO_4^{2-}	Ca^{2+}	Mg^{2+}	pH
Composition (mmol l^{-1})	376	343	33.5	6.4	2.3	4.1	1.5	7.7

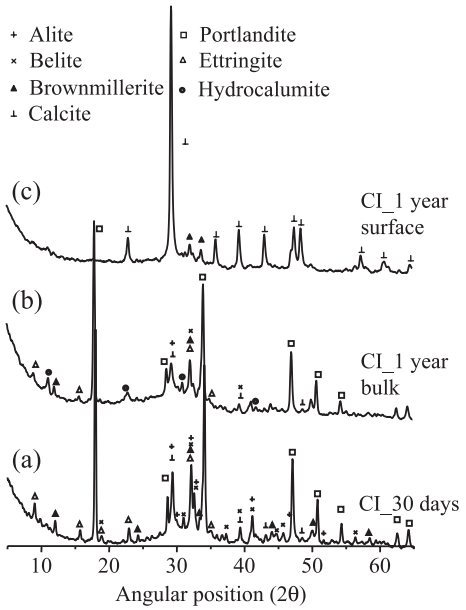

Fig. 1. XRD patterns of samples CI hydrated at T=293 K, p=10^5 Pa for (a) 30 days and (b, c) 1 year, $Cu_{K\alpha}$ radiation.

usual hydrated phases such as portlandite CH, and the AF_t phase ettringite $C_6A\bar{S}_3H_{32}$. The diffuse peak at 0.27–0.31 nm is attributable to C–S–H. After 1 year, XRD reveals that portlandite has been partially consumed and an AF_m phase hydrocalumite (also called Friedel's salt or chlorinated lamellar double hydroxide LDH) $[Ca_2Al(OH)_6]Cl\cdot 2H_2O$ appears (Fig. 1b). The AF_m family is composed of positively charged main layers $[Ca_4Al_2(OH)_{12}]^{2+}$ balanced by $2Cl^-$ and SO_4^{2-} anions, respectively, for Friedel's salt and monosulfate phase. At the surface, calcite $CaCO_3$ is the main crystalline material (Fig. 1c) due to carbonation.

In the CII samples cured at high temperature and high pressure for 30 days, ettringite phase was absent. Instead of ettringite, hydrogarnet C_3ASH_4 has been formed (Fig. 2a). Traditionally, the term hydrogarnet has been associated with minerals having a lower Si content than garnet C_3AS_3 due to the replacement of $(SiO_4)^{4-}$ by four $(OH)^-$. As a result, the composition may be described as a solid solution $C_3AS_{3-x}H_{2x}$ (where x=0–3). More recently, the term hydrogrossular has been applied to this solid solution [10] and so the terms hydrogarnet, Si-hydrogarnet and katoite are all referring to the same range of compositions. All phases are still present after 1 year (Fig. 2b) with a predominance of calcite at the surface (Fig. 2c). Interestingly, in both experiments, carbonation depth is minimal.

4.2. Magic angle spinning nuclear magnetic resonance spectroscopy

4.2.1. ^{29}Si MAS NMR

Fig. 3a shows the ^{29}Si NMR spectrum of unhydrated Class G cement. It contains a broad Q^0 component near −71 ppm, which is the sum of alite and belite. The observed line broadening arises from the incorporation of metal (Mg^{2+}, Al^{3+} and Fe^{3+}) and other impurity ions into the crystal lattice [11]. Two examples of the spectra decomposition are presented in Fig. 3b and e, respectively, for CI and CII samples after a 30-day cure. In each case, the spectra show resonances from the Q^0 units of the anhydrous cement with usual nonstoichiometric and noncrystalline calcium silicate hydrates (C–S–H). The main resonance lines at −79.2 and −85.5 ppm are respectively due to the end-chain tetrahedra Q^1 and nonbridging tetrahedra Q^2 of the C–S–H [12]. The peak for Q^2 sites is asymmetric or has a small shoulder at about −82.5 ppm. In calcium silicate hydrate, this peak has been already assigned to the middle tetrahedra of the dreierkette C–S–H chain structure (Q^2_L) (see Ref. [13] and references therein). However, in our samples, C–S–H also contains Al and the resonance at −82.5 ppm was also assigned to a Q^2(1Al) site by Richardson et al. [14] in a ^{29}Si MAS NMR investigation of a hydrated synthetic slag glass. The chemical shift of the resonance only observed as a shoulder near −90 ppm in CII samples is in the range for Q^2 and Q^3 units in calcium silicate hydrates [15]. This broad signal was observed for tobermorite formation process and assigned to Q^2 bridging tetrahedra which are connected by hydrogen bonding by Sato et al. [16]. In previous work on synthetic C–S–H [13], this signal is decomposed by two components Q^2_v and Q^3 respectively assigned to the Q^2 tetrahedra next to the Q^3 and to the Q^3 tetrahedra linking two silicates chains in the interlayer space. However, the chemical shift of these Q^3 units seems to be highly low field shift compared to the Q^3 chemical shift located near −96 ppm in

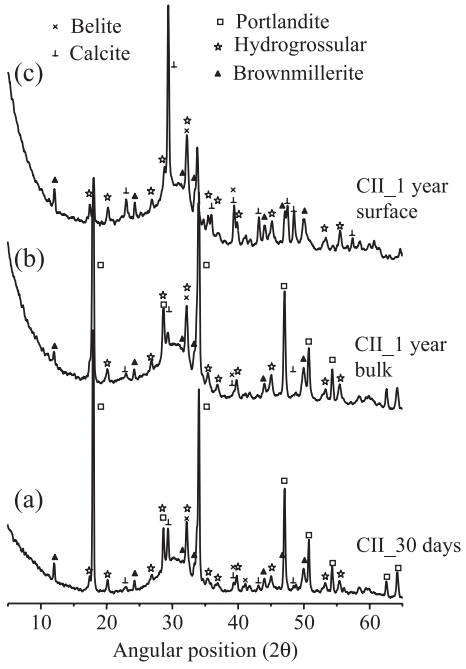

Fig. 2. XRD patterns of samples CII hydrated at T=353 K, p=7×10^6 Pa for (a) 30 days and (b, c) 1 year, $Cu_{K\alpha}$ radiation.

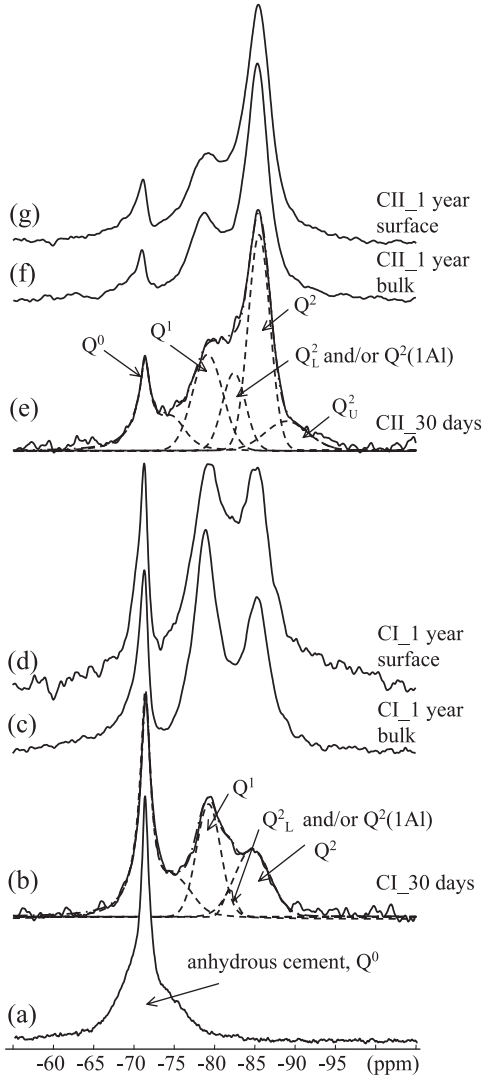

Fig. 3. ^{29}Si MAS NMR spectra of (a) anhydrous cement, samples hydrated at T=293 K, p=10^5 Pa for (b) 30 days and (c, d) 1 year and at T=353 K, p=7×10^6 Pa for (e) 30 days and (f, g) 1 year.

tobermorite [17]. Thus, its structure was not still clear but tentatively we assigned this signal to Q^2 units. The degree of hydration x and the average degree of C–S–H connectivity $\bar{n}$ are given by:

$$x = \frac{Q^1 + Q^2}{100}$$

$$\bar{n} = \frac{Q^1 + 2Q^2}{Q^1 + Q^2}$$

where the relative proportions of silicon associated with the Q^n units were determined by deconvolution of the spectra and measurement of the area associated with each peak using the dmfit program [18]. The results are reported in Table 2. Comparison of hydration of CI and CII samples for prolonged periods of time confirms the increasing degree of polymerisation $\bar{n}$ with curing time, temperature and pressure as shown by the increasing amount of Q^2 midchain units. As temperature and pressure increase, the degree of hydration x increases as shown by the decreasing relative intensity of the Q^0 peak. This is linked to an acceleration of the hydration kinetics with temperature and pressure, the Q^0 anhydrous species being transformed into calcium silicate hydrate (C–S–H). Such structural changes have been previously observed on hydration of tricalcium silicate at high temperatures and high pressure [19]. The ^{29}Si NMR spectra of the degraded layers after 1 year show an increase of Q^2_L and/or Q^2(1Al) compared to the bulk sample with a more pronounced effect in the CI sample whereas there is no or little difference between the spectra corresponding to surface and bulk of the $CII_{1\ year}$ specimen.

4.2.2. ^{27}Al MAS NMR

4.2.2.1. Anhydrous cement. For oilwell cements which contain a low bulk Al_2O_3/Fe_2O_3 ratio, the aluminate phase is usually present in very small quantities and Al is mainly in the ferrite phase. The ^{27}Al NMR spectrum for anhydrous oilwell cement (Fig. 4d) shows two main resonances at 80 and 6 ppm, indicative of tetrahedrally Al(IV) and octahedrally Al(VI) coordinated Al, respectively. Al(IV) resonance mostly arises from Al for Si substitution in the alite and belite phases [11], whereas octahedral sites may arise from small quantities of products formed during storage [6].

Skibsted et al. [20] show that Al present in the calcium aluminoferrites contributes little or no signal to the observed ^{27}Al MAS NMR spectrum because of ^{27}Al nucleus–Fe^{3+} unpaired electron dipolar couplings. However, ferrite phase composition is very variable and large variations in substitution can occur within an individual clinker as well as between clinkers of different overall compositions [21,22] leading to different ^{27}Al NMR spectra. Ferrite phase was

Table 2
Phases detected by XRD, ^{27}Al and ^{29}Si NMR

Class G Portland cement			
Hardened in tap water (30 days)		Exposed to brine (1 year)	
CI (T=293 K, p=10^5 Pa)	CII (T=353 K, p=7×10^6 Pa)	CI (T=293 K, p=10^5 Pa)	CII (T=353 K, p=7×10^6 Pa)
C_3S	C_3S	C_3S	C_3S
C_2S	C_2S	C_2S	C_2S
C_4AF	C_4AF	C_4AF	C_4AF
CH	CH	CH	CH
$C\bar{C}$	$C\bar{C}$	$C\bar{C}$	$C\bar{C}$
$C_4A\bar{S}H_{12}$	$C_4A\bar{S}H_{12}$	$C_4A\bar{S}H_{12}$	$C_4A\bar{S}H_{12}$
–	–	$[Ca_2Al(OH)_6]Cl\cdot 2H_2O$	–
$C_6A\bar{S}H_{32}$	–	$C_6A\bar{S}H_{32}$	–
–	C_3ASH_4	–	C_3ASH_4
C–S–H	C–S–H	C–S–H	C–S–H
bulk	bulk	bulk	bulk
$\bar{n}$=1.54, x=0.50	$\bar{n}$=1.73, x=0.80	$\bar{n}$=1.56, x=0.73	$\bar{n}$=1.77, x=0.86
		surface	surface
		$\bar{n}$=1.60, x=0.76	$\bar{n}$=1.77, x=0.85

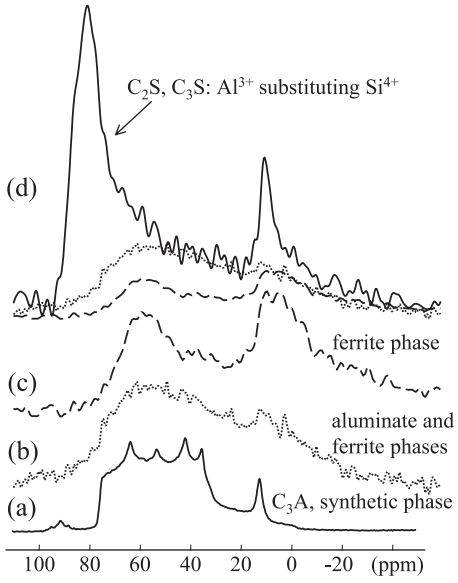

Fig. 4. ^{27}Al MAS NMR spectra of (a) synthetic phase C_3A, (b) anhydrous cement after salicylic acid treatment, (c) anhydrous cement after salicylic acid and sugar water treatments and (d) anhydrous cement.

separated from our anhydrous cement after dissolution of the silicate and aluminate phases respectively with salicylic acid–methanol solution and sugar water treatment [23]. XRD spectrum reveals only the brownmillerite C_4AF phase. The observation of tetrahedrally Al(IV) and octahedrally Al(VI) coordinated Al resonances with centres of gravity respectively at 60 and 6 ppm by ^{27}Al NMR (Fig. 4c) is in agreement with the ^{27}Al MAS NMR spectrum of synthetic ferrite phase $Ca_2Al_{0.93}Fe_{0.17}O_5$ from Skibsted et al. [20] that displays center of gravity for Al(IV) and Al(VI) respectively at 61 ppm and near 10 ppm (11.5 kHz spinning rate in a 9.4 T field). By comparing the ferrite spectrum to other spectra presented in this study, the observed severe loss of ^{27}Al NMR intensity in the ferrite phase show that Al present in the calcium aluminoferrites contributes little or no signal to the observed ^{27}Al MAS NMR spectrum. It is known that Fe in Portland cement does not migrate through the pore solution on hydration, but remains in products formed in situ [24], however, the extent to which Fe is incorporated into the hydrated phases is still debatable, but it is generally accepted that the A/F ratio of the C_4AF hydration products is greater than that of C_4AF itself [25]. We can also suppose that it may be possible to observe hydration products of ferrite phase by NMR experiments.

Although the aluminate phase is not revealed by XRD measurements, the difference between the NMR spectra of anhydrous cement after dissolution of silicate phases (Fig. 4b) and anhydrous cement after dissolution of silicate and aluminate phases (Fig. 4c) indicates its presence. Furthermore, the spectrum displayed on Fig. 4b overlaps well the spectrum of the synthetic sample of C_3A (see Ref. [26] for more details about the NMR spectrum of C_3A) and seems to indicate that the broad NMR signal around 20 and 80 ppm mainly originates from the aluminate phase. The lack of resolution may be ascribed to the incorporation of impurities ions in the crystal lattice.

4.2.2.2. CI samples (T=293 K, p=10^5 Pa). The ^{27}Al NMR spectra of CI cements are displayed on Figs. 5 and 6. On reaction with water, anhydrous cement initially forms ettringite $C_6A\bar{S}H_{32}$ (AF_t phase) and later the thermodynamically stable monosulfoaluminate $C_4A\bar{S}H_{12}$ (AF_m phase) which both contain exclusively octahedrally coordinated Al and lead to peaks in the ^{27}Al NMR spectra respectively near 13 and 10 ppm [27]. These phases are present in the $CI_{30\ days}$ sample. From the spectra in Fig. 6, it appears that the monosulfate resonance is reducing in intensity with curing time as a resonance located near 9 ppm grows. According to Jones et al. [28], this resonance may be attributed to the conversion of AF_m phase, monosulfate to Friedel's salt. These attributions are in agreement with XRD results that show an appearance of hydrocalumite (Friedel's salt) and a persistence of ettringite with curing time. As previously noticed, monosulfoaluminate phase is not detected by XRD indicating that the phase is poorly crystalline [24]. The spectra also yield signal in the Al(IV) range but, as reported in our previous study [6], the peak maximum has changed to about +65 from +82 ppm for the unhydrated cement. We only observed in the spectra the more shielded peak that arises from Al substituting Si in the C–S–H [11]. After 1 year, this peak is reducing in intensity in the core but is still intense at the surface. This indicates that chain lengthening observed between the core and surface of the $CI_{1\ year}$ sample by ^{29}Si

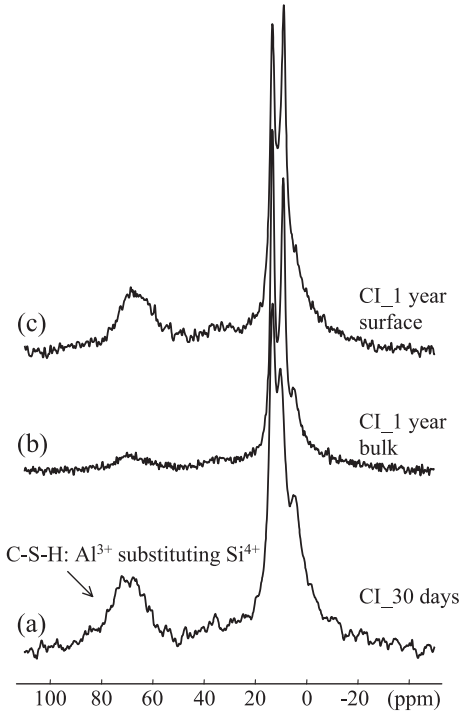

Fig. 5. ^{27}Al MAS NMR spectra of samples hydrated at T=293 K, p=10^5 Pa for (a) 30 days and (b, c) 1 year.

NMR, is rather due to incorporation of aluminium in the C–S–H (i.e., Q^2(1Al) units).

4.2.2.3. CII samples (T=353 K, p=7×10⁶ Pa). In sample $CII_{30\ days}$, a five-coordinated Al is detected near 36 ppm and tentatively assigned by Faucon et al. [29] to Al^{3+} substituting for Ca^{2+} ions located in the interlayer of the C–S–H structure (Fig. 7). The ^{27}Al NMR spectra reveal that ettringite phase was absent whereas monosulfate resonance is present. We can also notice the presence of a band at 5 ppm and a broad band near −20 ppm. The broadest line near −20 ppm has been attributed to hydrogrossular phases [30]. The large width of this band can be explained by the highly distortion of site because of Si-site partial substitution by OH and Al-site by iron. This attribution is in agreement with XRD results that show the presence of hydrogrossular phases in the CII sample. In all samples, we can observe a peak near 5 ppm which is not clearly assigned. According to Porteneuve et al. [31], this resonance may be attributed to the hydrogarnet phase but in the investigation of aluminium incorporation in the C–S–H, this peak has been assigned to Al^{3+} substituting Ca^{2+} in the octahedral sheet of the C–S–H structure [29,32]. However Andersen et al. [33] believe, from ^{27}Al–{^{1}H} CP/MAS NMR experiments, that this resonance originates from a separate phase, most likely a less crystalline alumina phase or a calcium aluminate hydrate including $Al(OH)_6^{3-}$ or $O_xAl(OH)_{6-x}^{(3+x)-}$ octahedra. Another approach to simplify spectra, often used with XRD experiments before Rietveld quantification, is to perform chemical extraction. XRD (not shown) and ^{27}Al NMR spectra of $CII_{30\ days}$ sample after extraction of silicates using salicylic acid in methanol show the dissolution of the silicate phases C_2S and C–S–H whereas hydrogrossular and ferrite phases are still present (Fig. 7). The disappearance of the resonances at 5 and 36 ppm may confirm the attribution to Al incorporated in the C–S–H, however, salicylic acid extraction also dissolves some aluminate phase as ettringite so further studies are needed for peaks assignments. The spectra of the sample after dissolution also contain a band near 55 ppm that is clearly in the range for Al(IV) that cannot be attributed to Al in the ferrite or C–S–H phases.

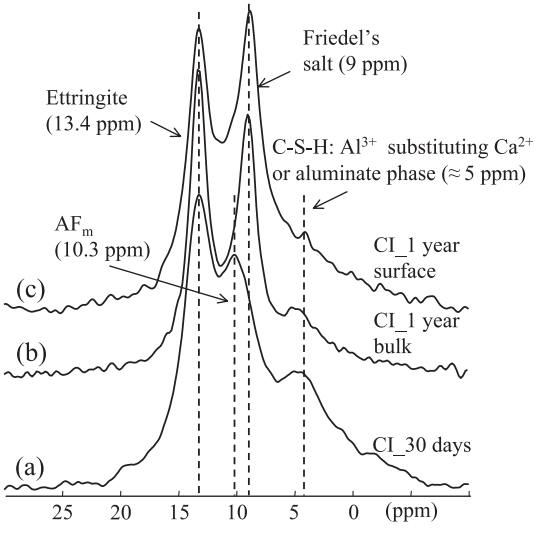

Fig. 6. ^{27}Al NMR spectra of samples hydrated at T=293 K, p=10^6 Pa for (a) 30 days and (b, c) 1 year.

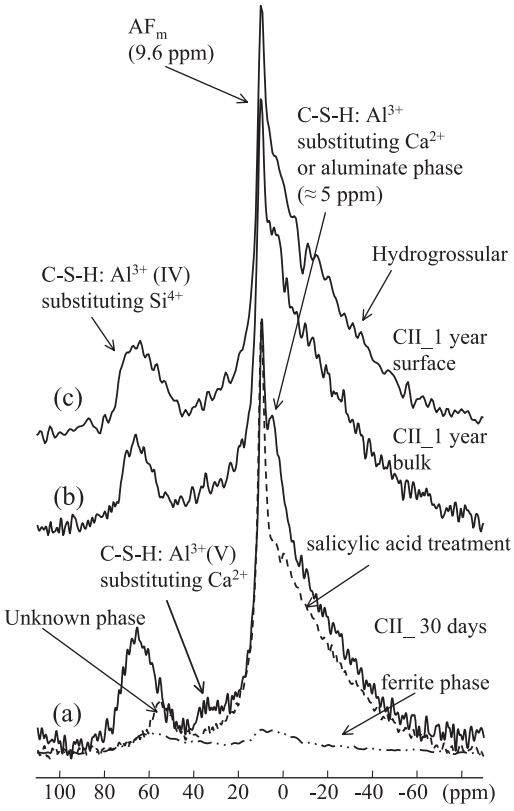

Fig. 7. ^{27}Al MAS NMR spectra of samples hydrated at T=353 K, p=7×10^6 Pa for (a) 30 days and (b, c) 1 year.

5. Discussion

The main products of hydration of Portland-based oilwell cement Class G exposed to brine with two curing temperature and pressure conditions are summarized in Table 2.

5.1. CI samples (T=293 K, p=10⁵ Pa)

CI samples contain both monosulfate and ettringite but after 1 year of immersion in brine (see Table 1 for chemical composition), conversion of the AF_m phase, monosulfate to Friedel's salt is observed in both XRD and NMR results. The mechanism of Friedel's salt formation may occur by the conversion of hydroxyl-AF_m by ion exchange and/or by the absorption of Cl^- from solution by precipitation [34]. Jones et al. [28] have considered dissolution/reprecipitation as well as ion exchange and

their results indicate that the ion exchange of chloride with hydroxide ions in monosulfate is dominant, at least at ages of up to 50 days.

The diffraction spectra of the surface layers indicate that leaching resulted in the disappearance of portlandite. When the cement paste with a pore solution of pH comprised between 12 and 13 is placed in contact with the brine, concentration gradients form within the pore solution. They will cause dissolution and precipitation phenomena of the solid phase, which are no longer in equilibrium with the pore solution [35]. In the degraded zone, there is a decalcification of the paste. Portlandite dissolves thereby maintaining the calcium concentration of the pore solution. But the main phenomenon responsible of portlandite dissolution is carbonation. $CO_2(g)$ dissolves to give $CO_2(aq)$ which then equilibriates: $CO_2(g)+2OH^-(aq)\leftrightarrow CO_3^{2-}(aq)+H_2O$. This carbon dioxide dissolution induces the dissolution of the hydrated phases, like portlandite, followed by the precipitation of calcium carbonate according to the reaction: $Ca(OH)_2(s)+CO_3^{2-}(aq)\leftrightarrow CaCO_3(s)+H_2O(aq)$. This is consistent with XRD measurements which showed the presence of calcite at the surface of the cement specimen. Indeed, XRD spectra indicate that cement exposed to brine develops a surface skin consisting mainly of calcite due to the saturation of the solution at the cement/brine interface with calcium carbonate. Thermodynamic calculations indicate that pure calcite is the stable form of calcium carbonate and the magnesium level in our solution is too low compared to Mg content of sea water (respectively around 50 and 1.5 mmol l^{-1}) to permit the precipitation of brucite (magnesium hydroxide) and aragonite in preference to calcite. It is important to note that our solution is not constantly renewed enhancing the precipitation of carbonates on the surfaces that may create a self-healing effect that reduces the leaching process [36].

Leaching of cement pastes also results in polymerisation of the C–S–H. This chain lengthening is accompanied by marked incorporation of aluminium in the C–S–H as previously observed by Faucon et al. [37] in a cement paste leached by deionized water. However, the source of aluminium incorporated in C–S–H is still questionable.

5.2. CII samples ($T=353$ K, $p=7\times10^6$ Pa)

In the samples cured at high temperature and high pressure, XRD and NMR results show that the ettringite phase was absent, instead hydrogrossular has been formed. In cement paste, ettringite normally decomposes at about 343 K, whereas crystallization of hydrogrossular is accelerated in autoclaved cement. According to Paul et al. [38], the alumina, present at ambient temperature in AF_t, is instead incorporated into other phases, notably hydrogrossular. Taylor has reported previous studies in Portland cement indicating hydrogrossular had formed by hydration of the ferrite [24]. This can lead to a high level of substitution of aluminium by iron in the hydrogrossular phase that can explain the important width of its ^{27}Al NMR resonance.

The C–S–H composition is markedly affected by the curing conditions. The polymerisation of the C–S–H structure increases with temperature and pressure. Such modifications in the hydrates structure may be linked to a change in the Ca/Si ratio. Even if the rate of hydration increases with temperature and pressure, the average degrees of connectivity of the C–S–H in sample I did not reach those obtained in sample II. However, after 30 days, the degree of hydration and the average degree of C–S–H connectivity in sample II seem near the maximum and slowly increase with curing time. Contrarily to the ^{29}Si NMR results of sample I, the spectra of sample II after 1 year of curing in brine reveal no or little change between the structure of the C–S–H in the core and in the surface. The diffraction spectra of the surface layers indicate that leaching only resulted in the disappearance of portlandite and formation of calcite in the surface. Contrary to what one could observe with sample I, the diffuse peak attributable to C–S–H between 0.27 and 0.31 nm is still present at the surface of the sample II.

6. Conclusion

Class G oilwell cements with two curing conditions were analysed by XRD and NMR measurements. The sample cured at $T=293$ K, $p=10^5$ Pa during 30 days has a normal mineralogy and microstructure: Unhydrated cement persists and the matrix consists of Portlandite, ettringite, monosulfate and C–S–H. After 1 year of immersion in brine, monosulfate is converted to Friedel's salt. Leaching resulted in the disappearance of portlandite and the formation of calcite and a more polymerised C–S–H. In the $T=353$ K, $p=7\times10^6$ Pa mineralogy, ettringite is converted to hydrogrossular and the average degree of connectivity of the C–S–H structure is increased.

Although the Fe content of oilwell cement is quite large, reasonable well-defined NMR spectra can be obtained from phases except ferrite. In order to have a better understanding of the ^{27}Al NMR spectra, selective dissolution has been performed and reveals a band in the range for Al(IV) not yet attributed. Further studies aimed at elucidating the structure of this aluminate phase are in progress. Furthermore, mechanical tests and porosity measurements are in progress to try to establish a correlation between the structure and macroscopic properties.

Acknowledgements

The authors would like to thank Institut Français du Pétrole for the permission to publish this paper. They are grateful to Annie Audibert-Hayet for valuable discussions, and Bernadette Rebours, Sylvie Massot, Isabelle Clémençon for their help in XRD measurements.

References

[1] I. Barclay, J. Pallenbarg, F. Tettero, J. Pfeiffer, H. Slater, T. Staal, D. Stiles, G. Tilling, C. Whitney, The beginning of the end: a review of abandonment and decommissioning practices, Oilfield Rev. 13 (2001) 28–41.

[2] E. Grabowski, J.E. Gillot, Effect of replacement of silica flour with silica fume on engineering properties of oilwell cements at normal and elevated temperatures and pressures, Cem. Concr. Res. 19 (1989) 333–344.

[3] C. Noïk, A. Rivereau, C. Vernet, Novel cements materials for high-pressure/high-temperature wells, Paper SPE 50589 presented at the SPE European Petroleum Conference, The Hague, The Netherlands, 20–22 October, 1998.

[4] C. Noïk, A. Rivereau, Oilwell cement durability, Paper SPE 56538 presented at the SPE Annual Technical Conference and Exhibition, Houston, TX, 3–6 October, 1999.

[5] Z. Krilov, B. Loncaric, Z. Miksa, Investigation of a long-term cement deterioration under a high-temperature, sour gas downhole environment, Paper SPE 58771 presented at the SPE International Symposium on Formation Damage Control, Lafayette, LA, 23–24 February, 2000.

[6] G. Le Saoût, E. Lécolier, A. Rivereau, H. Zanni, Study of oilwell cements by solid state NMR, C. R., Chim. 7 (2004) 383–388.

[7] M.B. Dusseault, M.N. Gray, P.A. Nawrocki, Why oilwells leak: cement behaviour and long-term consequences, Paper SPE 64733 presented at the SPE International Oil and Gas Conference and Exhibition, Beijing, China, 7–10 November, 2000.

[8] J.S. Lota, J. Bensted, P.L. Pratt, Characterisation of an unhydrated Class G oilwell cement, I.I, Cemento 729 (1998) 172–183.

[9] G. Engelhardt, D. Michel, High-Resolution Solid-State NMR of Silicates and Zeolites, Wiley, New York, 1987.

[10] E. Passaglia, R. Rinaldi, Katoite, a new member of the $Ca_3Al_2(SiO_4)_3$–$Ca_3Al_2(OH)_{12}$ series and a new nomenclature for hydrogrossular group of mineral, Bull. Minéral. 107 (1984) 605–618.

[11] J. Skibsted, H.J. Jakobsen, P. Colombet, A.-R. Grimmer, Characterization of the calcium silicate and aluminate phases in anhydrous and hydrated portland cements, in: P. Colombet, A.-R. Grimmer, H. Zanni, P. Soozzani (Eds.), Nuclear Magnetic Resonance Spectroscopy of Cement-Based Materials, Springer, Berlin, 1998, pp. 3–45.

[12] G.M. Bell, J. Bensted, F.P. Glasser, E.E. Lachowski, D.R. Roberts, M.J. Taylor, Study of calcium silicate hydrates by solid state high resolution ^{29}Si nuclear magnetic resonance, Adv. Cem. Res. 3 (1990) 23–37.

[13] I. Klur, B. Pollet, J. Virlet, A. Nonat, C–S–H structure evolution with calcium content by multinuclear NMR, in: P. Colombet, A.-R. Grimmer, H. Zanni, P. Soozzani (Eds.), Nuclear Magnetic Resonance Spectroscopy of Cement-Based Materials, Springer, Berlin, 1998, pp. 119–141.

[14] I.G. Richardson, A.R. Brough, R. Brydson, G.W. Groves, C. Dobson, Location of aluminium in substituted calcium silicate hydrate (C–S–H) gels as determined by ^{29}Si and ^{27}Al NMR and EELS, J. Am. Ceram. Soc. 76 (1993) 2285–2288.

[15] A.-R. Grimmer, Structural investigation of calcium silicates from ^{29}Si chemical shift measurements, in: P. Colombet, A.-R. Grimmer (Eds.), Application of NMR Spectroscopy to Cement Science, Gordon and Breach, Amsterdam, 1994, pp. 113–151.

[16] H. Sato, M. Grutzek, Effect of starting materials on the synthesis of Tobermorite, Mater. Res. Soc. Symp. Proc. 245 (1992) 235–240.

[17] W. Wieker, A.-R. Grimmer, A. Winkler, M. Mägi, T. Tarmak, E. Lippmaa, Solid-state high resolution ^{29}Si NMR spectroscopy of synthetic 14 Å, 11 Å and 9 Å Tobermorites, Cem. Concr. Res. 12 (1982) 333–339.

[18] D. Massiot, F. Fayon, M. Capron, I. King, S. Le Calvé, B. Alonso, J.O. Durand, B. Bujoli, Z. Gan, G. Hoatson, Modelling one- and two-dimensional solid-state NMR spectra, Magn. Reson. Chem. 40 (2002) 70–76.

[19] B. Bresson, F. Méducin, H. Zanni, C. Noik, Hydration of tricalcium silicate (C_3S) at high temperature and high pressure, J. Mater. Sci. 37 (2002) 1–11.

[20] J. Skibsted, H.J. Jakobsen, C. Hall, Quantitative aspects of ^{27}Al MAS NMR of calcium aluminoferrites, Adv. Cem. Based Mater. 7 (1998) 57–59.

[21] C. Hall, K.L. Scrivener, Oilwell cement clinkers X-ray microanalysis and phase composition, Adv. Cem. Based Mater. 7 (1998) 28–38.

[22] I.G. Richardson, C. Hall, G.W. Groves, TEM study of the composition of the interstitial phase in an oil-well cement clinker, Adv. Cem. Res. 5 (1993) 15–21.

[23] L.P. Lejbina, Quantitative analysis of tricalcium aluminate and tetracalcium aluminoferrite in the same sample, Ogneupory SSSR 34 (1969) 52–56.

[24] H.F.W. Taylor, Cement Chemistry, Thomas Telford Publishing, London, 1997.

[25] N. Meller, C. Hall, A.C. Jupe, S.L. Colston, S.D.M. Jacques, P. Barnes, J. Phipps, The paste hydration of brownmillerite with and without gypsum: a time resolved synchrotron diffraction study at 30, 70, 100 and 150 °C, J. Mater. Chem. 14 (2004) 428–435.

[26] D. Müller, W. Gessner, A. Samoson, E. Lippmaa, G. Scheller, Solid-State NMR studies on polycrystalline aluminates of the system CaO–Al_2O_3, Polyhedron 5 (1986) 779–785.

[27] J. Skibsted, E. Henderson, H.J. Jacobsen, Characterization of calcium aluminate phases in cements by ^{27}Al MAS NMR spectroscopy, Inorg. Chem. 32 (1993) 1013–1027.

[28] M.R. Jones, D.E. Macphee, J.A. Chudek, G. Hunter, R. Lannegrand, R. Talero, S.N. Scrimgeour, Studies using ^{27}Al MAS NMR of AF_m and AF_t phases and the formation of Friedel's salt, Cem. Concr. Res. 33 (2003) 177–182.

[29] P. Faucon, A. Delagrave, J.C. Petit, C. Richet, J.M. Marchand, H. Zanni, Aluminium incorporation in calcium silicate hydrates (C–S–H) depending on their Ca/Si ratio, J. Phys. Chem., B 103 (1999) 7796–7802.

[30] P. Faucon, J.F. Jaquinot, F. Adenot, N. Gautier, D. Massiot, J. Virlet, ^{27}Al MAS NMR study on cement paste degradation by water, in: P. Colombet, A.-R. Grimmer, H. Zanni, P. Soozzani (Eds.), Nuclear Magnetic Resonance Spectroscopy of Cement-Based Materials, Springer, Berlin, 1998, pp. 403–409.

[31] C. Porteneuve, H. Zanni, C. Vernet, K.O. Kjellsen, J.P. Korb, D. Petit, Nuclear magnetic resonance characterization of high- and ultrahigh-performance concrete application to the study of water leaching, Cem. Concr. Res. 31 (2001) 1887–1893.

[32] H. Stade, D. Müller, G. Scheler, ^{27}Al-NMR-spektroskopische Untersuchungen zur Koordination des Al in C–S–H (Di, Poly), Z. Anorg. Allg. Chem. 510 (1984) 16–24.

[33] M.D. Andersen, H.J. Jakobsen, J. Skibsted, Incorporation of aluminium in the silicate hydrate (C–S–H) of hydrated portland cements: a high-field ^{27}Al and ^{29}Si MAS NMR investigation, Inorg. Chem. 42 (2003) 2280–2287.

[34] A.K. Suryavanshi, J.D. Scantlebury, S.B. Lyon, Mechanisms of Friedel's salt formation in cements rich in tricalcium aluminate, Cem. Concr. Res. 26 (1996) 717–727.

[35] F. Adenot, B. Gérard, J.M. Torrenti, Etat de l'art, in: J.M. Torrenti, O. Didry, J.P. Ollivier, F. Plas (Eds.), La Dégradation Des Bétons, Hermes Science Publications, Paris, 1999, pp. 19–45.

[36] C. Vernet, C. Alonso, C. Andrate, M. Castellote, I. Llorente, A. Hidalgo, A new leaching test based in a running water system to evaluate long-term water resistance of concretes, Adv. Cem. Res. 14 (2002) 157–168.

[37] P. Faucon, F. Adenot, J.F. Jacquinot, J. Virlet, R. Cabrillac, M. Jorda, Contribution of nuclear magnetic resonance techniques to the study of cement paste water degradation, in: H. Justnes (Ed.), Proceedings of the 10th International Congress on the Chemistry of Cement, Gothenburg (Sweden), 1997, pp. 3v003.

[38] M. Paul, F.P. Glasser, Impact of prolonged warm (85 °C) moist cure on Portland cement paste, Cem. Concr. Res. 30 (2000) 1869–1877.